Small composite field correction factors for the CyberKnife radiosurgery system: clinical and PCSR plans

Christiansen, Eric Jessie; Muir, Bryan Richard; Belec, Jason; Vandervoort, Eric J.

Publisher's version / Version de l'éditeur:
https://doi.org/10.1088/1361-6560/aa954c
Physics in Medicine and Biology, 2017-11

Small composite field correction factors for the CyberKnife radiosurgery system: clinical and PCSR plans

E Christiansen[1,2] (present affiliation), B Muir[3], J Belec[4] and E Vandervoort[4]

[1] McGill University, Montreal, QC, H3A 0G4, Canada
[2] Carleton University, Ottawa, ON, K1S 5B6, Canada
[3] Measurement and Science Standards, National Research Council of Canada, Ottawa, ON, K1A 0R6, Canada
[4] The Ottawa Hospital Cancer Centre, Ottawa, ON, K1H 8L6, Canada

E-mail: ericchristiansen@cmail.carleton.ca

June 2017

Abstract. A formalism has been proposed for small and non-standard photon fields in which $k^{f_{\text{clin}},f_{\text{msr}}}_{Q_{\text{clin}},Q_{\text{msr}}}$ correction factors are used to correct dosimeter response in small fields (indiviual or composite) relative to that in a larger machine-specific reference (MSR) field. For clinical plans consisting of several fields, a plan-class specific reference (PCSR) plan can also be defined, serving as an intermediate calibration field between the MSR and clinical plans within a certain plan-class. In this work, the formalism was applied in the calculation of $k^{f_{\text{clin}},f_{\text{msr}}}_{Q_{\text{clin}},Q_{\text{msr}}}$ for 21 clinical plans delivered by the CyberKnife radiosurgery system, each plan employing one or two of the smallest diameter collimators: 5 mm, 7.5 mm, and 10 mm. Three detectors were considered: the Exradin A16 and A26 micro chambers, and the W1 plastic scintillator. The clinical plans were grouped into 7 plan-classes according to commonly shared characteristics. The suitability of using a plan-class specific reference (PCSR) plan to represent the detector response of each plan within the plan-class was investigated. Total and intermediate correction factors were calculated using the `egs_chamber` Monte Carlo user code. The corrections for the micro chambers were large, primarily due to the presence of the low-density air cavity and the volume averaging effect. The correction for the scintillator was found to be close to unity for most plans, indicating that this detector may be used to measure small clinical plan correction factors in any plan except for those using the 5 mm collimator. The PCSR plan was shown to be applicable to plan-classes comprising isocentric plans only, with plan-classes divided according to collimator size. For non-isocentric plans, the variation of $k^{f_{\text{clin}},f_{\text{msr}}}_{Q_{\text{clin}},Q_{\text{msr}}}$ as a function of the point of measurement within a single plan, as well as the high inter-plan-class variability of the correction factor, precludes the use of a PCSR plan.

Submitted to: *Phys. Med. Biol.*

1. Introduction

Small fields and the use of non-standard delivery techniques are increasingly being employed in stereotactic ablative radiosurgery, with the aim of treating smaller lesions with a high dose while sparing nearby radiosensitive organs. In order to correctly interpret the relationship between dose and tumour response and complications using different radiosurgery systems, a high level

of mechanical and dosimetric accuracy is required (Benedict et al. 2010). In particular, detectors calibrated in large reference fields according to current protocols (e.g., TG51 (Almond et al. 1999) and its addendum (McEwen et al. 2014), TRS-398 (Andreo et al. 2000)) may require substantial correction factors when measuring the dose-to-water in small fields, defined to be fields for which the lateral electron range is larger than the dimensions of the field size (Das et al. 2008). This implies that lateral charged particle equilibrium (CPE) is not achieved at any point within the field. When a dosimeter with a density substantially different than its surrounding medium is used to measure the dose to that medium (e.g., an air-filled ionization chamber in water), large perturbations to the electron fluence (and the dose) are observed for small fields (Bouchard et al. 2015). Volume-averaging effects are also observed when the detector's sensitive volume is large compared to the field size.

A formalism for small and non-standard field dosimetry has been introduced in order to account for detector-specific perturbations to the measured dose in clinical plans in which dosimeter response differs from that in the reference field (Alfonso et al. 2008) (we use the word plan to denote a delivery consisting of a collection of individual fields). Correction factors $k^{f_{\text{clin}},f_{\text{ref}}}_{Q_{\text{clin}},Q_{\text{ref}}}$ are defined as the ratio of dose-to-water and detector reading in the clinical field divided by the same ratio evaluated in the standard $100 \times 100\,\text{mm}^2$ reference field. If the machine is incapable of producing such a field, a machine-specific reference (MSR) field is used instead, taken to be the largest available field (e.g., 60 mm diameter circular field for CyberKnife). This formalism has been applied extensively for individual field configurations, with several authors having calculated $k^{f_{\text{clin}},f_{\text{msr}}}_{Q_{\text{clin}},Q_{\text{msr}}}$ correction factors in small individual fields (Cranmer-Sargison et al. 2012, Ralston et al. 2012, Scott et al. 2012, Czarnecki & Zink 2013, Bassinet et al. 2013, Azangwe et al. 2014, Benmakhlouf et al. 2014, Francescon, Beddar, Satariano & Das 2014, Francescon, Kilby & Satariano 2014, Moignier et al. 2014, Barrett & Knill 2016).

The formalism defines a second set of correction factors for plans, which requires grouping clinical plans that share some similarity into plan-classes. A plan-class specific reference (PCSR) plan is then selected or constructed to represent the plan-class. According to the original definition, this plan should deliver a uniform dose over a region extending past the detector (Alfonso et al. 2008); it should also have the same characteristics that were used to define the plan-class. A detector calibrated in the PCSR plan may then be used to measure the dose-to-water in any plan in the class. In order to ensure that this can be done without further correction, the correction factors $k^{f_{\text{clin}},f_{\text{msr}}}_{Q_{\text{clin}},Q_{\text{msr}}}$ and $k^{f_{\text{pcsr}},f_{\text{msr}}}_{Q_{\text{pcsr}},Q_{\text{msr}}}$ should be similar; this is equivalent to the statement that the correction factor from the PCSR to the clinical field $k^{f_{\text{clin}},f_{\text{pcsr}}}_{Q_{\text{clin}},Q_{\text{pcsr}}}$ is close to unity. Comparatively little work has been done calculating correction factors for patient plans using multiple fields: Gago-Arias et al. (2013) found no correlation between correction factors for two CyberKnife clinical plans and two PCSR plans using the same set of collimators as the respective clinical plan.

In this paper, we calculate the $k^{f_{\text{clin}},f_{\text{msr}}}_{Q_{\text{clin}},Q_{\text{msr}}}$ correction factors for 21 clinical CyberKnife plans composed of multiple fields employing small collimators. Calculations are done for two air filled micro chambers and a plastic scintillator detector (PSD). Due to the near water equivalence of the material used in its construction (Beddar et al. 1992*a*, Beddar et al. 1992*b*, Francescon, Kilby & Satariano 2014), the use of the PSD as a correction-free dose-to-water dosimeter in small clinical plans is investigated. These correction factors are calculated using Monte Carlo simulations: detailed models of the CyberKnife unit and the three detectors are constructed. Analysis is aided

by decomposing the full correction factor into intermediate correction factors, each one attributable to a different non-water component of the detector (Bouchard et al. 2009). We also explore the suitability of using a representative PCSR plan to represent a class of clinical plans.

2. Materials and Methods

2.1. Beam modelling

The CyberKnife (Accuray, Sunnyvale, CA) linac head (G4 model) was modelled in detail in BEAMnrc (Rogers et al. 1995) according to technical drawings provided by the manufacturer. A low-energy particle production threshold of `AE`=512 keV and `AP`=1 keV for knock-on electrons and bremsstrahlung photons, respectively, was selected for each material. Low-energy particle transport thresholds of `ECUT`=512 keV and `PCUT`=10 keV for charged particles and photons, respectively, were used throughout the BEAMnrc simulation of the linac head. The EGSnrc (Kawrakow 2000, Kawrakow & Rogers 2000) particle transport settings were set to the BEAMnrc default values. Bremsstrahlung cross-section enhancement (Ali & Rogers 2007) and directional bremsstrahlung splitting (Kawrakow et al. 2004) were used to increase the efficiency of the BEAMnrc simulations.

After each component of the linac head was modelled, the energy and spatial characteristics of the modelled electron beam incident on the target were matched to measured data by tuning the energy and full width at half maximum (FWHM) parameters, respectively. The parameter estimation was done by comparing measurements and calculations of the percentage depth-dose (PDD), off-axis ratio (OAR), and output factors (OF) assessed using the χ^2 statistic. All calculations were done using the `egs_chamber` (Wulff et al. 2008) user code; a detailed model of the measuring detector was created in `egs_chamber`, including the manufacturer's specifications for the stem, central electrode, wall, and air cavity. This allows for the direct comparison between measurements and calculations without the application of correction factors, since all perturbative effects, such as the finite size of the detector, are directly included in the calculations (Sheikh-Bagheri & Rogers 2002, Francescon et al. 2008, Almberg et al. 2012, Gago-Arias et al. 2013, Papaconstadopoulos et al. 2014).

The BEAMnrc linac model was used as a particle source for the `egs_chamber` simulation. Low-energy particle transport thresholds of `ECUT`=512 keV and `PCUT`=10 keV for charged particles and photons, respectively, were used throughout the `egs_chamber` simulations. The EGSnrc particle transport settings were set to the `egs_chamber` default values. Intermediate phase-space storage (IPSS) (Chibani & Ma 2007, Wulff et al. 2008), correlated sampling (CS) (Ma & Nahum 1993, Buckley et al. 2004, Wulff et al. 2008), and photon cross-section enhancement (XCSE) (Wulff et al. 2008) variance reduction techniques were used in the `egs_chamber` simulations. The IPSS and XCSE regions were set to surround the detector.

2.1.1. Beam data measurements All measurements of the CyberKnife beam data for the purposes of tuning the beam model were done with the Exradin A16 ionization chamber (Standard Imaging, Middleton, WI), having a nominal collecting volume of 7 mm^3 (2.4 mm diameter). The chamber was placed in the IBA Blue Phantom 2 scanning water tank (IBA Dosimetry, Schwarzenbruck, Germany), oriented with the stem perpendicular to the beam central axis. An IBA FC-65G Farmer-

type ionization chamber was used as a reference chamber for these measurements, placed at the edge of the field defined by the primary collimator in the linac head, in order to track and correct for variations in linac output.

The PDD for the 60 mm collimator was measured from 300 mm below the water surface to 10 mm above. No shift of the effective point of measurement was considered, since all detector materials were fully modeled in the calculations. The normalization at 50 mm depth was done by fitting the falloff region of the measured PDD (starting at a depth of 30 mm) to a fourth order polynomial (Sheikh-Bagheri & Rogers 2002). Off-axis ratios (OARs) for the three smallest collimators (5 mm, 7.5 mm, and 10 mm) were measured at three depths each: 15 mm, 50 mm, and 200 mm. Each OAR was centred and symmetrised before comparing to calculated data (Papaconstadopoulos et al. 2014). OF measurements were performed at an SSD of 785 mm, with the depth of the detector fixed at 15 mm. OFs for the same set of collimators were measured, with the 60 mm collimator used as the reference field. A Fluke electrometer, model number 35040, was used for the OF measurements instead of the IBA electrometer, because of its thresholding features and minimal leakage currents. Measurements for each collimator were made using a polarizing voltage of −300 V. Corrections for the polarity effect (OFs only) and a radiation-induced background signal present in the scanning water tank electrometer (Ali 2016) (PDD and OARs only) were measured using the A16 chamber and the Fluke electrometer in a Gammex certified therapy grade Solid Water slab geometry. The corrections for the radiation-induced background signal amounted to changes of less than three percentage points in the PDD and OARs.

2.2. Plan Correction Factors

2.2.1. Monte Carlo calculations for plans Clinical plan measurements for the CyberKnife unit at The Ottawa Hospital Cancer Centre (TOHCC) are performed in a custom solid water phantom. This phantom is approximately head-shaped: a hemisphere attached to a cylinder of the same radius. Additional components are composed of either stainless steel, polyoxymethylene, or PMMA. A fully detailed model of the phantom was constructed in `egs_chamber`, including all non-solid water components. The plans were modeled in `egs_chamber` using a procedure similar to that described by Ma et al. (2008). Details about the plans generated by the CyberKnife treatment planning system are stored in XML files, which were converted to field angles and weights understood by the `egs_chamber` user code. The same `egs_chamber` settings and cut-off energies were used for the correction factor calculation and beam modelling. IPSS, CS, and XCSE variance reduction techniques were also used, with the IPSS and XCSE regions set to surround each detector. Simulations were run until a $< 0.2\%$ statistical uncertainty in the dose to detector was achieved.

2.2.2. Total correction factor calculation The clinical plan correction factors were calculated for three different detectors: the Exradin A16 and A26 micro chambers, and the W1 PSD (Standard Imaging, Middleton, WI); characteristics of each of these detectors are listed in Table 1. Each detector was modelled in `egs_chamber` at a fixed position inside the phantom, with the centroid of the sensitive volume of each detector at the same point inside the phantom. A separate geometry was defined, in which a sphere of water with radius 0.3 mm was placed within the solid water phantom at this same position; this geometry is necessary in order to calculate the numerators in

Table 1. Size of the sensitive volume and material composition of certain components of the three detectors used in this study. The final column lists the electrode material for the ion chambers, and the scintillating material for the PSD.

Detector	Nominal sensitive volume (mm^3)	Wall	Electrode/scintillator
A16	7	C-552	Aluminum
A26	15	C-552	C-552
W1	2	ABS	Polysterene

the $k^{f_{\rm clin},f_{\rm msr}}_{Q_{\rm clin},Q_{\rm msr}}$ and $k^{f_{\rm pcsr},f_{\rm msr}}_{Q_{\rm pcsr},Q_{\rm msr}}$ correction factors:

$$k^{f_{\rm clin},f_{\rm msr}}_{Q_{\rm clin},Q_{\rm msr}} = \frac{D^{f_{\rm clin}}_{w,Q_{\rm clin}}/M^{f_{\rm clin}}_{Q_{\rm clin}}}{D^{f_{\rm msr}}_{w,Q_{\rm msr}}/M^{f_{\rm msr}}_{Q_{\rm msr}}} \approx \frac{D^{f_{\rm clin}}_{w,Q_{\rm clin}}/D^{f_{\rm clin}}_{det,Q_{\rm clin}}}{D^{f_{\rm msr}}_{w,Q_{\rm msr}}/D^{f_{\rm msr}}_{det,Q_{\rm msr}}} \quad (1a)$$

$$k^{f_{\rm pcsr},f_{\rm msr}}_{Q_{\rm pcsr},Q_{\rm msr}} = \frac{D^{f_{\rm pcsr}}_{w,Q_{\rm pcsr}}/M^{f_{\rm pcsr}}_{Q_{\rm pcsr}}}{D^{f_{\rm msr}}_{w,Q_{\rm msr}}/M^{f_{\rm msr}}_{Q_{\rm msr}}} \approx \frac{D^{f_{\rm pcsr}}_{w,Q_{\rm pcsr}}/D^{f_{\rm pcsr}}_{det,Q_{\rm pcsr}}}{D^{f_{\rm msr}}_{w,Q_{\rm msr}}/D^{f_{\rm msr}}_{det,Q_{\rm msr}}}. \quad (1b)$$

The first part of Equations (1*a*) and (1*b*) is the definition of each correction factor; the second half represents the approximation that the relation between the corrected detector reading $M^{f_{\rm clin}}_{Q_{\rm clin}}$ and the absorbed dose-to-detector $D^{f_{\rm clin}}_{det,Q_{\rm clin}}$ is independent of beam quality or field size. Therefore we are calculating the relative absorbed-dose energy dependence $f(Q)^{f_{\rm clin},f_{\rm msr}}_{Q_{\rm clin},Q_{\rm msr}}$ (Rogers 2009); for simplicity, we will call this the total correction factor $k^{f_{\rm clin},f_{\rm msr}}_{Q_{\rm clin},Q_{\rm msr}}$ for the remainder of the paper. We emphasize that the quantity $M^{f_{\rm clin}}_{Q_{\rm clin}}$ is the detector reading in field $f_{\rm clin}$ corrected for all environmental effects and other measurement effects, which may be non-trivial for these detectors in small fields. These corrections include polarity and ion recombination for the micro chambers (McEwen 2010), as well as Cerenkov light contamination for the PSD (Guillot et al. 2011).

Dose was scored within the sensitive volume of each detector, as well as the water sphere, in order to compute the dose ratio $D^{f_{\rm clin}}_{w,Q_{\rm clin}}/D^{f_{\rm clin}}_{det,Q_{\rm clin}}$ and $D^{f_{\rm pcsr}}_{w,Q_{\rm pcsr}}/D^{f_{\rm pcsr}}_{det,Q_{\rm pcsr}}$. A similar method was used to calculate the $D^{f_{\rm msr}}_{w,Q_{\rm msr}}/D^{f_{\rm msr}}_{det,Q_{\rm msr}}$ ratio, present in the denominator of the $k^{f_{\rm clin},f_{\rm msr}}_{Q_{\rm clin},Q_{\rm msr}}$ and $k^{f_{\rm pcsr},f_{\rm msr}}_{Q_{\rm pcsr},Q_{\rm msr}}$ correction factors, for the 60 mm MSR field.

2.2.3. Intermediate correction factor calculation The chain of intermediate volumes defined by Bouchard et al. (2009), from fully modelled detector to a small volume of water, was used to calculate the intermediate correction factors $P_{\rm stem}$ (if required), $P_{\rm cel}$, $P_{\rm wall}$, $\left(\frac{\overline{L}}{\rho}\right)^{w}_{det}$ $P_{\rm repl}$, P_ρ, and $P_{\rm vol}$. These intermediate correction factors will aid in the analysis of the full $k^{f_{\rm clin},f_{\rm msr}}_{Q_{\rm clin},Q_{\rm msr}}$ in Section 4. In general, a component is removed by replacing its material with its surrounding medium. In the case of the ion chambers, the central electrode is therefore replaced with air. All other detector components are replaced with the phantom material, in this case Solid Water (see Section 2.2.1 for a description of the phantom used in the clinical plan calculations). A 0.3 mm radius sphere, placed at the centroid of the detector sensitive volume, was used as the small volume of water.

The perturbation factor associated with a detector component (stem, central electrode, and wall) is given by the ratio of the dose scored in the sensitive volume with and without that component removed. The final perturbation factors are given by changing the bare sensitive volume to the

sphere of water in three steps: (1) the sensitive volume is changed to a volume filled with water with the same density as the active material ($\left(\frac{\overline{L}}{\rho}\right)^{w}_{det} P_{\text{repl}}$); (2) the density of water in the sensitive volume is changed to the correct density for water (P_ρ); and (3) the sensitive volume of water is changed to a small sphere of water (P_{vol}). In this final simulation, we effectively calculate dose to water in Solid Water.

These perturbations factors are computed for the three detectors, in each clinical and PCSR plan, as well as the MSR field. For each detector component, c, the intermediate correction factors are defined as ratios of the corresponding perturbation factors in the plans and the MSR field: $[P_c]^{f_{\text{clin}},f_{\text{msr}}}_{Q_{\text{clin}},Q_{\text{msr}}}$ and $[P_c]^{f_{\text{pcsr}},f_{\text{msr}}}_{Q_{\text{pcsr}},Q_{\text{msr}}}$ for the clinical and PCSR plans, respectively. The product of all the intermediate correction factors yields the total correction factor $k^{f_{\text{clin}},f_{\text{msr}}}_{Q_{\text{clin}},Q_{\text{msr}}}$ for that plan.

2.2.4. Clinical Plan-Classes A total of 21 clinical plans, all of which have been used for patient treatments at TOHCC, were sorted into seven plan-classes of three plans each. The clinical plans were grouped according to shared characteristics, which are shown in Table 2. Plan-classes are defined by which collimator(s) are used, the anatomy treated, the set of source positions available for treatment (referred to as field paths), and the shape of the resulting dose distribution. Both isocentric (ISO) and non-isocentric (NONISO) delivery types were investigated. Only plans utilizing one to two of the three smallest (5 mm, 7.5 mm, and 10 mm diameter) collimators were investigated.

Clinical plans within the isocentric plan-classes (ISO-5mm, ISO-7.5mm and ISO-10mm) are used to treat small spherical metastases using the head field path (the head path refers to a pre-defined set of CyberKnife field positions for cranial treatments). The size of the collimator is selected to provide optimal target coverage. Clinical plans within plan-classes NONISO-TN1 and NONISO-TN2 treat an approximately 6 mm length of the trigeminal nerve in patients with trigeminal neuralgia (TN), a severe chronic pain disorder. Both NONISO-TN1 and NONISO-TN2 use non-isocentric delivery and a specialized TN field path. NONISO-TN1 uses only the 5 mm collimator, while NONISO-TN2 uses both 5 and 7.5 mm collimators. Finally, clinical plans within plan-class NONISO-AN1 and NONISO-AN2 are used to treat patients with small volume (approximately 500 to 1000 mm^3) acoustic neuroma (AN), a benign usually slow-growing tumor of the vestibulocochlear nerve. Plan-classes NONISO-AN1 and NONISO-AN2 employ non-isocentric delivery, the head field path and use 5 and 7.5 mm collimators but have different dose distribution characteristics.

Non-isocentric clinical plans, especially those using multiple collimators, can yield irregularly shaped dose distributions, in which the centre of the target receives less dose than the periphery. This is possible because the field directions for a non-isocentric plan are selected by keeping the source positions fixed and directing the field central axes at randomly distributed points (referred to as targets) on the surface of the target volume, causing a subset of the fields to intersect at the periphery of the target. Each clinical plan in plan-class NONISO-AN2 was of the type that produced this irregular dose distribution. The clinical plans in plan-classes NONISO-TN1, NONISO-TN2 and NONISO-AN1 as well as the isocentric clinical plan-classes (ISO-5mm, ISO-7.5mm and ISO-10mm), yield dose distributions in which the centre of the target receives a larger dose than the periphery.

2.2.5. PCSR plans PCSR plans were created for each set of clinical plans which employed a unique delivery type (isocentric or non-isocentric), field path (trigeminal neuralgia or head path), and the

Table 2. The seven clinical plan-classes investigated. Each plan-class is named according to characteristics defining the clinical plans within that class. These characteristic include: isocentric (ISO) or Non-isocentric (NONISO) delivery; acoustic neuroma (AN) or trigeminal neuralgia (TN) treatment type; and the collimator size(s) that is (are) used.

Plan-class name	Delivery type	Field path	Collimator(s) (mm)
ISO-5mm	Isocentric	Head	5
ISO-7.5mm	Isocentric	Head	7.5
ISO-10mm	Isocentric	Head	10
NONISO-TN1	Non-isocentric	TN	5
NONISO-TN2	Non-isocentric	TN	5 & 7.5
NONISO-AN1	Non-isocentric	Head	5 & 7.5
NONISO-AN2	Non-isocentric	Head	5 & 7.5

set of collimator(s) used to define the plan. Therefore, all plan-classes in Table 2 have unique PCSRs except NONISO-AN1 and NONISO-AN2.

For the isocentric plan-classes, PCSR plans were constructed using every source position available for the particular path represented, with each field having equal weight (i.e., MU). This can be compared to clinical isocentric plans, in which certain source positions have been excluded, and the field weights have been optimized to improve target coverage and to avoid radiosensitive organs. The requirement that the PCSR plan provide a uniform dose over a volume extending over the dimensions of the detector (Alfonso et al. 2008), is not fulfilled in the isocentric PCSR plans. In order to create a low-dose gradient region using small collimators in CyberKnife, a non-isocentric plan would have to be used, in which field penumbrae overlap. Such a PCSR plan, however, would no longer be representative of isocentric clinical plans, therefore the requirement of dose uniformity was relaxed.

The PCSR plans for non-isocentric plan-classes were constructed to provide a more uniform dose distribution by using fields directed at target points randomly distributed on the outer and inner surface of a set of five 1 mm thick concentric spherical shells surrounding the centre of the detector active volume. The field weights for all PCSR plans were optimized using the same plan template in the CyberKnife planning system (MultiPlan version 4.6.0). Sequential optimization was used without relaxed convergence, using an optimize coverage constraint of 9.5 Gy and a maximum allowed dose of 10.5 Gy for the entire target volume (union of the detector sensitive volume and shell structures). The total monitor units (MU) per plan was 35000, the maximum MU per beam was 100, and no limit was set for the maximum MU per node. These plans provide a relatively homogeneous dose (approximately ± 5%) extending isotropically several mm from the centroid of the detector active volume. In contrast, the clinical plans have much more heterogeneous dose distributions with variations in dose within the target region approximately between ± 10% to ± 15%. Examination of the suitability of these homogeneous PCSR plans to provide correction factors for heterogeneous clinical plans can be found in Section 4.

The intra-plan-class variability of total and intermediate correction factors was assessed for all the clinical plans assigned to each plan-class. For a group of clinical plans within a proposed plan-class, a variation between calculated $k_{Q_{\mathrm{clin}},Q_{\mathrm{msr}}}^{f_{\mathrm{clin}},f_{\mathrm{msr}}}$ of less than 1% was considered ideal, with a maximum variation of 2% tolerated. In addition, the values of the $k_{Q_{\mathrm{clin}},Q_{\mathrm{pcsr}}}^{f_{\mathrm{clin}},f_{\mathrm{pcsr}}}$ for each plan-class were

examined; a maximum departure of 2% from unity was deemed acceptable for a candidate PCSR plan to represent the plan-class. These figures were selected by considering that the component of the uncertainty in the determination of the dose-to-water in small clinical plans related to the omission of the $k_{Q_{\text{clin}},Q_{\text{pcsr}}}^{f_{\text{clin}},f_{\text{pcsr}}}$ should only make up a fraction of the total uncertainty of approximately 2-4% recommended in the AAPM reports for dosimetric accuracy in IMRT (Ezzell et al. 2003) and for robotic radiosurgery (Dieterich et al. 2011).

2.2.6. The MSR field The clinical field correction factors are defined relative to a suitable MSR field. The MSR field for the CyberKnife unit was taken to be the 60 mm collimator (Alfonso et al. 2008); the detectors were placed perpendicular to the field at a depth in water of 50 mm and at a source to detector distance (SDD) of 800 mm, (phantom dimensions: $300 \times 300 \times 500\,\text{mm}^3$).

2.2.7. Detector position For single fields, the detector-specific correction factors $k_{Q_{\text{clin}},Q_{\text{msr}}}^{f_{\text{clin}},f_{\text{msr}}}$ depend on the field of interest, as well as the position of the detector within the field, with the off-axis position having a larger effect on the correction factor than the depth or SDD (Francescon, Beddar, Satariano & Das 2014). Clinical plans in CyberKnife consist of many individual fields superimposed on one another, therefore in general, the $k_{Q_{\text{clin}},Q_{\text{msr}}}^{f_{\text{clin}},f_{\text{msr}}}$ should depend on detector position for these plans as well. In light of this, a standard procedure must be followed to select the detector position within the clinical plans, so that differences between the $k_{Q_{\text{clin}},Q_{\text{msr}}}^{f_{\text{clin}},f_{\text{msr}}}$ for different plans are not due to detector placement, but to the plan properties.

For all isocentric PCSR and clinical plans, the centroid of the detector volume was selected to be at the point of intersection of all of the field central axes. Two points of measurement were assessed for non-isocentric clinical plans. The first point considered was the point of maximum dose. However, this point may be situated in a region of high dose gradient, whereas the PCSR plan was constructed to have a low dose gradient in a volume surrounding the point of measurement. In order to find a measurement point in the clinical plan with dosimetric conditions as similar as possible to the PCSR plan, the dose gradient in a region surrounding the detector should be as low as possible. To that end, for each point $\vec{r}$, a metric $I(\vec{r})$ was constructed, being equal to the magnitude of the normalized dose gradient integrated over a sphere of radius 2 mm centred at $\vec{r}$:

$$I(\vec{r}) = \int_{|\vec{r}-\vec{r}'|\leq 2\,\text{mm}} \left| \frac{\vec{\nabla} D(\vec{r}')}{D(\vec{r}')} \right| \mathrm{d}^3\vec{r}'. \tag{2}$$

This metric was minimized with respect to the point $\vec{r}$, subject to the constraint that the dose at the optimal dose gradient metric point is greater than 80% of the maximum dose. Correction factors for the non-isocentric plans were calculated at both the maximum dose point and the optimal dose gradient metric point. The 2 mm radius was selected so that the integrated volume encompassed the entire sensitive volume of all detectors considered.

3. Results

3.1. Beam modelling

The electron beam incident on the target was estimated to have a total energy of 6.7 MeV and a FWHM of 2.5 mm. Following a procedure similar to Almberg et al. (2012), the final energy was

Table 3. Uncertainty budget for the measured and Monte Carlo calculated dose distribution data. Errors due to detector position assume a position uncertainty of 0.2 mm. Errors due to uncertainties in the detector modelling and the underlying photon cross sections are shown only for the OFs. Shown in the table are values for a specific point in these data. For the 60 mm PDD, this point was at a depth $z = 50$ mm. The uncertainties for both the OAR and OF are evaluated for the 5 mm collimator. Uncertainty in the OAR is shown at a radius $r = 3$ mm from central axis (radius of 50% dose), in the large-gradient penumbra region, hence the large uncertainty due to detector positioning.

		Type A	Type B		Total
		Statistical	Combined detector modelling[a] and cross section[b]	Detector position	
PDD	Measurement	0.13%		0.23%	0.26%
	Calculation	0.82%			0.82%
OAR	Measurement	0.22%		10%	10%
	Calculation	0.15%			0.15%
OF	Measurement	0.21%		0.50%	0.54%
	Calculation	0.15%	0.56%		0.58%

[a] (Francescon et al. 2011)
[b] (Muir & Rogers 2010)

determined by minimizing the slope and intercept ($-0.00217\,\%$/mm and $-0.363\,\%$, respectively) of the line of best fit of the deviation between the measured and calculated PDDs in the 60 mm collimator. Figure 1 shows the direct comparison between the PDD measured with the A16 micro chamber and the PDD calculated using the final initial electron energy of 6.7 MeV, both normalized to 100% at a depth of 50 mm. An uncertainty budget for example points in the measured and calculated PDDs, OARs, and OFs is provided in Table 3.

Using a 2.5 mm FWHM initial electron beam gave the best overall agreement when comparing calculated and measured OAR and OFs as determined using the χ^2 statistic. The χ^2 value was minimized at a FWHM of 2.5 mm for the OAR of the 7.5 mm collimator; for the OARs of the remaining collimators, and the OFs, the value of χ^2 divided by the number of degrees of freedom is less than 1, and within 0.25 of the minimal value. Figure 2 and Table 4 show the direct comparison between the small field OARs and OFs measured with the A16 micro chamber and the respective simulations, calculated using the initial electron energy and FWHM of 6.7 MeV and 2.5 mm, respectively.

Good agreement within uncertainties between measurements and calculations is observed for the PDD and the small field OARs and OFs using these initial electron beam parameters (χ^2 per degree of freedom less than 1), indicating that this model may be used to calculate detector correction factors in small fields.

3.2. Plan Correction Factors

3.2.1. Isocentric clinical plan-classes The total correction factors relative to the MSR field for the three clinical plans and the PCSR plan within the isocentric plan-classes are presented in Figure 3. The error bars represent the estimated statistical uncertainty in the calculated correction factors.

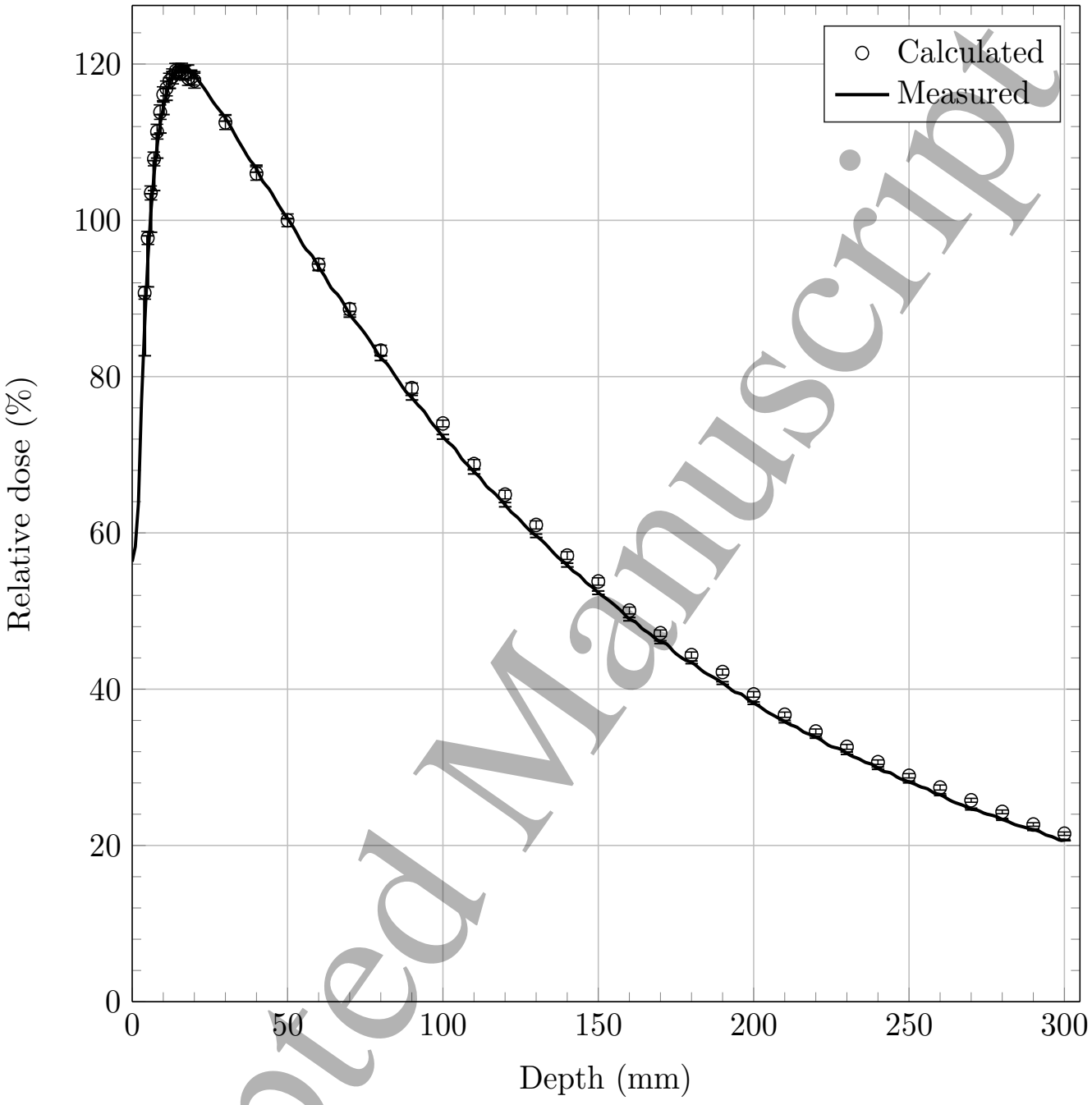

Figure 1. Comparison between the PDD for the 60 mm collimator measured using the A16 micro chamber and the corresponding Monte Carlo calculations using a full source and detector model (optimized electron beam parameters: $E = 6.7\,\mathrm{MeV}$, $\mathrm{FWHM} = 2.5\,\mathrm{mm}$).

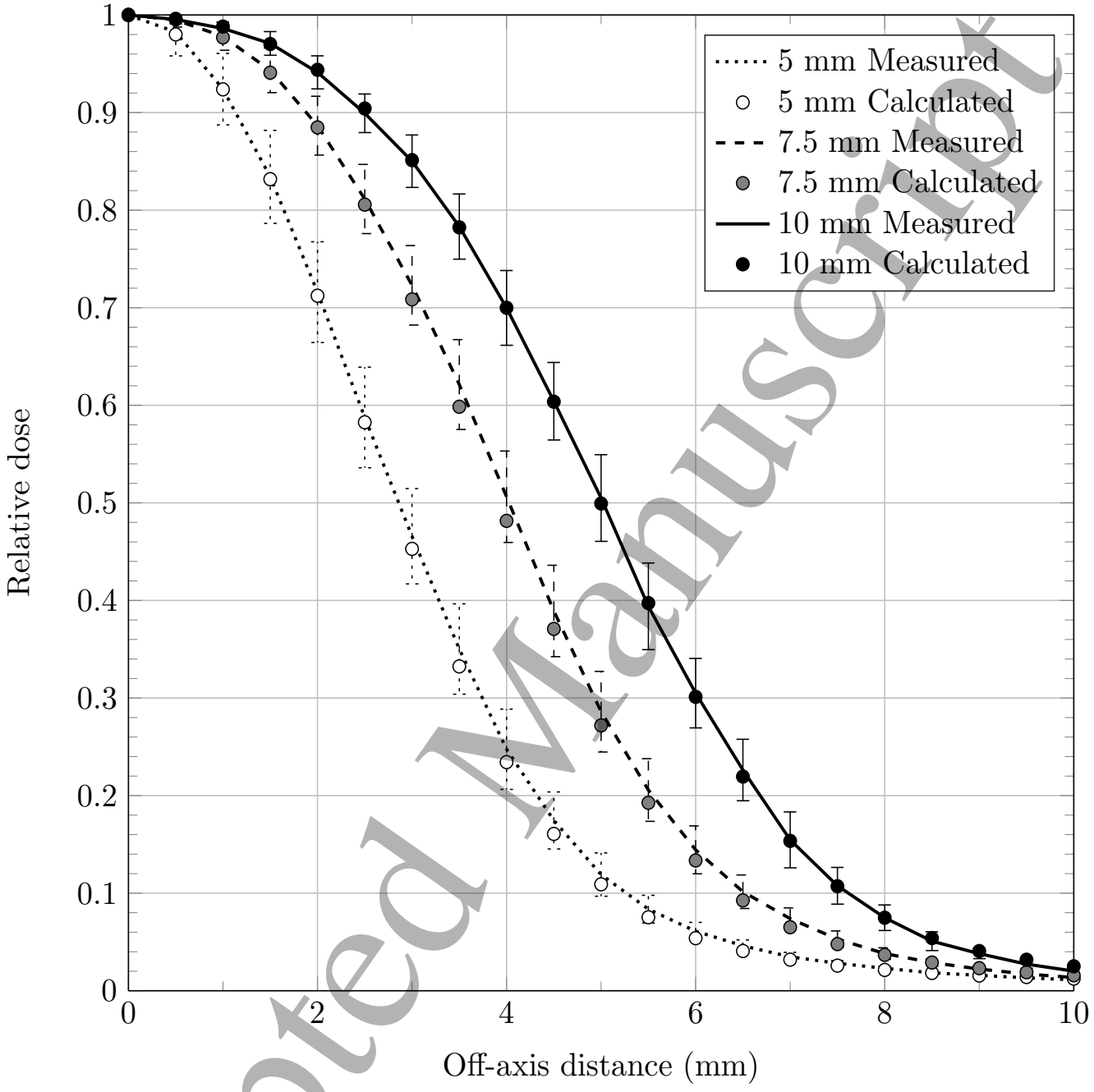

Figure 2. Comparison between small field OARs at a depth of 15 mm, measured using the A16 micro chamber, and the corresponding Monte Carlo calculations using a full source and detector model (optimized electron beam parameters: $E = 6.7$ MeV, FWHM = 2.5 mm). The error bars for the calculated values are approximately the same size as the circles.

Table 4. Comparison between small field OFs, measured using the A16 micro chamber, and the corresponding Monte Carlo calculations using a full source and detector model (optimized electron beam parameters: $E = 6.7\,\mathrm{MeV}$, FWHM $= 2.5\,\mathrm{mm}$). Note that no correction factors are applied to the measurements, since a full model of the source and detector were used for the calculations. Uncertainties in the last digit are given in parentheses.

Collimator (mm)	Measured	Calculated
5	0.581(3)	0.574(3)
7.5	0.783(4)	0.782(5)
10	0.844(4)	0.853(5)

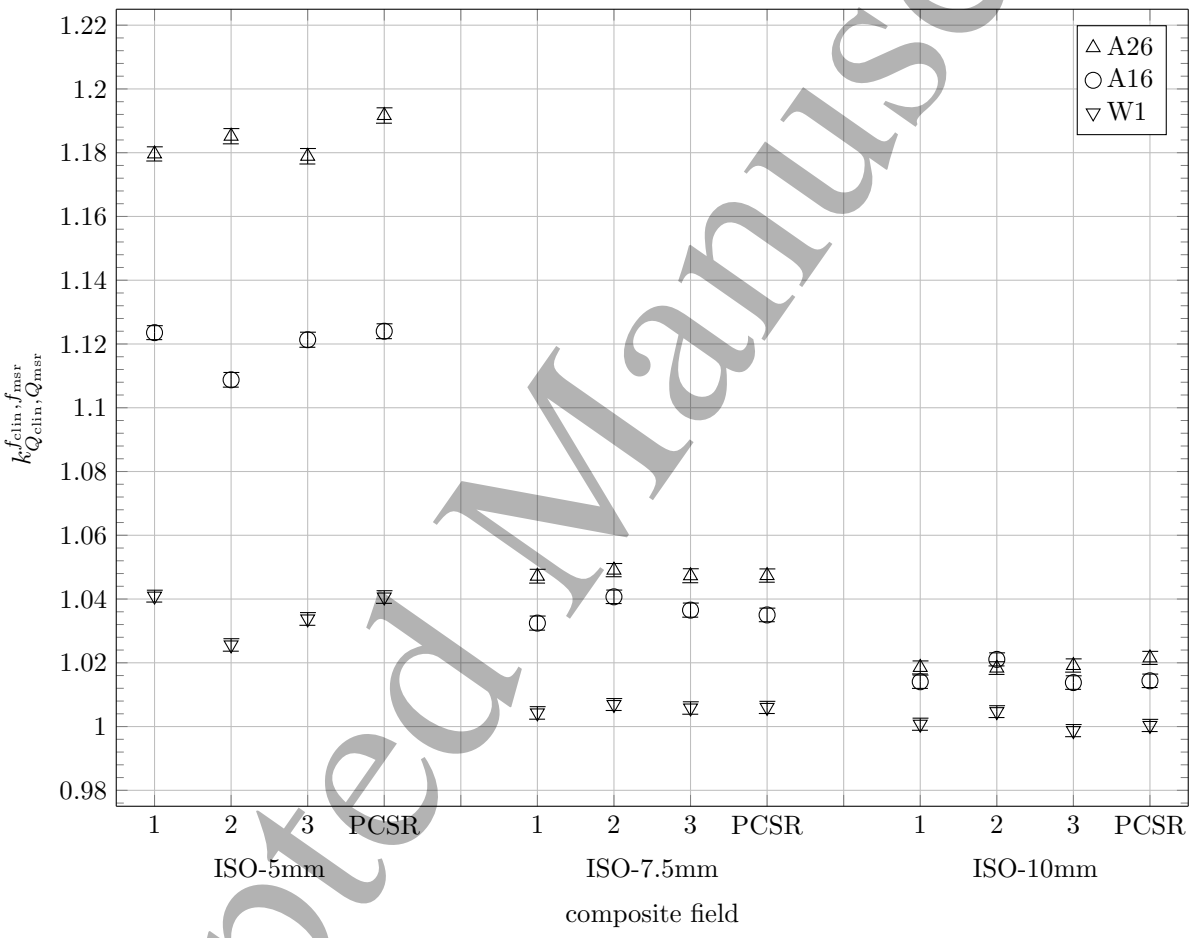

Figure 3. Total $k^{f_{\mathrm{clin}},f_{\mathrm{msr}}}_{Q_{\mathrm{clin}},Q_{\mathrm{msr}}}$ correction factors for isocentric clinical and PCSR plans, grouped according to plan-class.

The intermediate correction factors were calculated for the PCSR plan representing the isocentric plan-classes. The intermediate correction factors for the clinical plan in each plan-class are within 1.5% of the corresponding intermediate correction factor for the PCSR field representing that plan-class. Results for PCSR ISO-5mm plan are shown in Figure 4; the results for the remaining plan-classes have a similar structure, but smaller values relative to unity as the collimator size is increased. In general, the behaviour of the $k^{f_{\mathrm{clin}},f_{\mathrm{msr}}}_{Q_{\mathrm{clin}},Q_{\mathrm{msr}}}$ is dominated by the volume averaging and density correction factors.

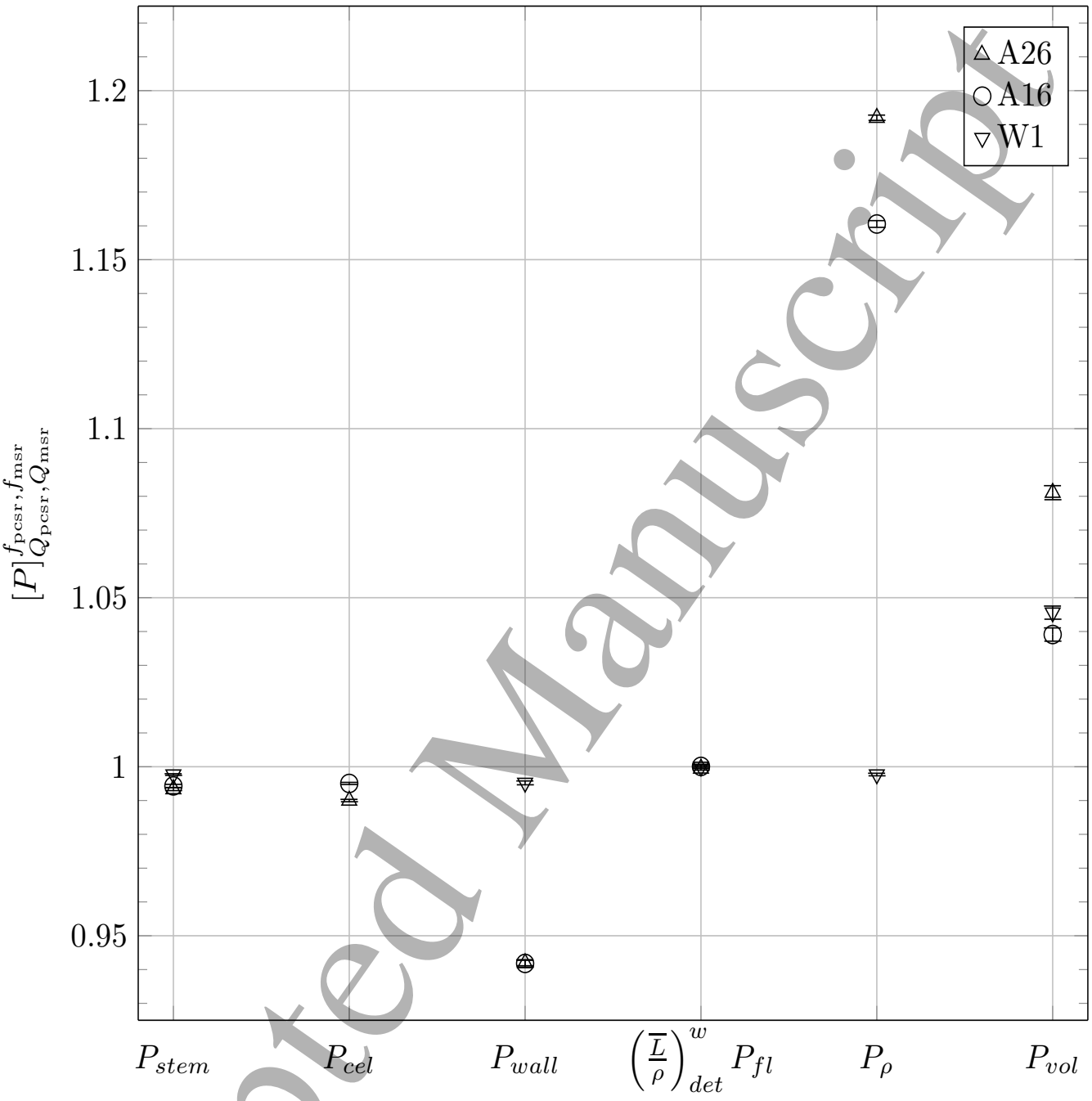

Figure 4. Intermediate correction factors $[P_c]^{f_{\mathrm{pcsr}},f_{\mathrm{msr}}}_{Q_{\mathrm{pcsr}},Q_{\mathrm{msr}}}$ for the representative PCSR plan of isocentric plan-class ISO-5mm.

3.2.2. Non-isocentric clinical plan-classes The total correction factors for the clinical and PCSR plans within each plan-class are presented in Figure 5. $k^{f_{\mathrm{clin}},f_{\mathrm{msr}}}_{Q_{\mathrm{clin}},Q_{\mathrm{msr}}}$ correction factors were calculated at two points within each clinical plan. The point of maximum dose coincides with the optimal dose gradient metric point $\vec{r}_{I_{min}}$ for each plan within plan-class NONISO-TN1; only one point of measurement is considered for the PCSR plans: the centre of the homogenous dose region.

As in the isocentric plans, $k^{f_{\mathrm{clin}},f_{\mathrm{msr}}}_{Q_{\mathrm{clin}},Q_{\mathrm{msr}}}$ is almost completely determined by the volume averaging and density correction factors. Only these correction factors are shown, therefore, in Figure 6; only

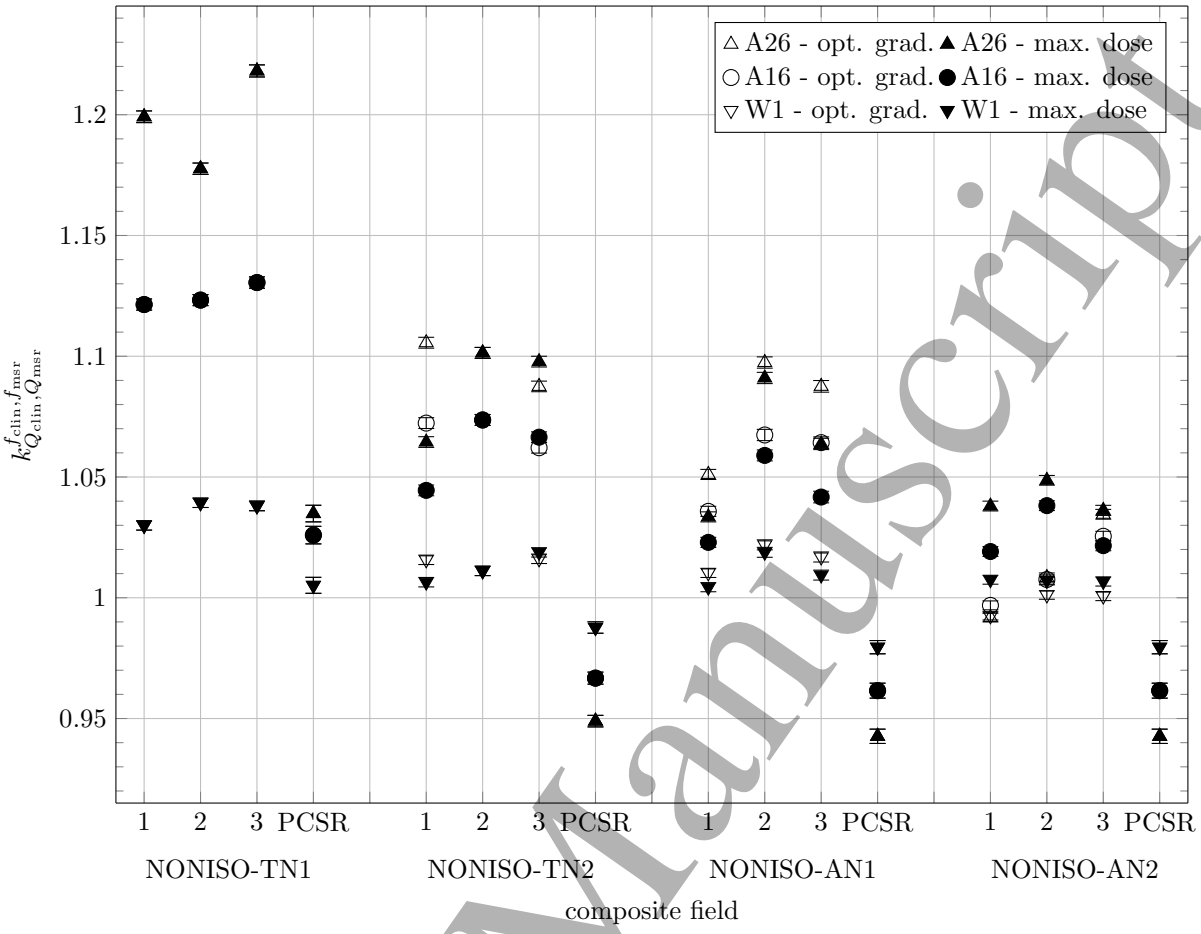

Figure 5. Total $k^{f_{\mathrm{clin}},f_{\mathrm{msr}}}_{Q_{\mathrm{clin}},Q_{\mathrm{msr}}}$ correction factors for non-isocentric clinical plans, calculated at the optimal dose gradient metric point and the maximum dose point, grouped according to plan-class.

data for the A16 is shown to represent correction factors for an intermediate detector with sensitive volume size between the two extremes of the A26 and W1.

A summary of the total correction factors for each plan-class for the A16 microchamber is shown in Table 5. The plan-classes which satisfy the candidate PCSR plan requirements, as well as the PCSR plans which satisfy the plan-class representation requirements, are indicated.

4. Discussion

4.1. Isocentric clinical plan-classes

The $k^{f_{\mathrm{clin}},f_{\mathrm{pcsr}}}_{Q_{\mathrm{clin}},Q_{\mathrm{pcsr}}}$ correction factors (ratios of $k^{f_{\mathrm{clin}},f_{\mathrm{msr}}}_{Q_{\mathrm{clin}},Q_{\mathrm{msr}}}$ to $k^{f_{\mathrm{pcsr}},f_{\mathrm{msr}}}_{Q_{\mathrm{pcsr}},Q_{\mathrm{msr}}}$) are within 1.4%, 0.5%, and 0.7% of unity for each isocentric clinical plan using the 5 mm, 7.5 mm, and 10 mm collimators, respectively, indicating that the chosen PCSR plans fulfill the requirement (at the 2% level) that it be representative of clinical plans within its class (see Table 5).

In general, the $k^{f_{\mathrm{clin}},f_{\mathrm{msr}}}_{Q_{\mathrm{clin}},Q_{\mathrm{msr}}}$ correction factors were larger for the A26 than for the A16 micro chamber, both requiring corrections greater than unity. The largest magnitude intermediate correction factors for both the A16 and A26 micro chambers are the density and volume averaging correction factors, agreeing with the small field results on central axis from several

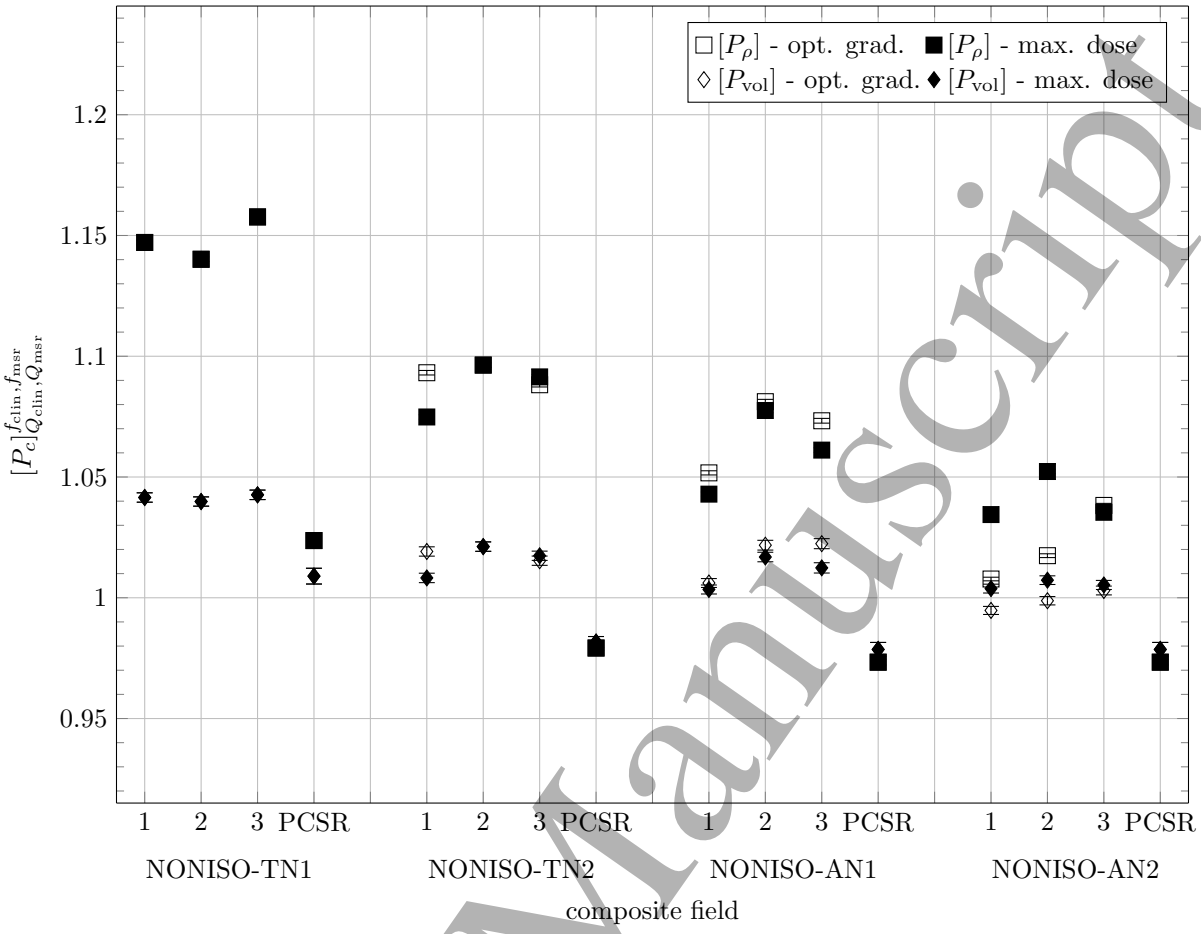

Figure 6. $[P_\rho]^{f_{\mathrm{clin}},f_{\mathrm{msr}}}_{Q_{\mathrm{clin}},Q_{\mathrm{msr}}}$ and $[P_{\mathrm{vol}}]^{f_{\mathrm{clin}},f_{\mathrm{msr}}}_{Q_{\mathrm{clin}},Q_{\mathrm{msr}}}$ intermediate correction factors for non-isocentric clinical plans, shown as diamonds and squares, respectively, at the optimal and maximum dose points for the A16 detector.

Table 5. Summary of total correction factors for the A16 microchamber, by plan-class. $\left|\Delta k^{f_{\mathrm{clin}},f_{\mathrm{msr}}}_{Q_{\mathrm{clin}},Q_{\mathrm{msr}}}\right|$ refers to the spread of the intra-plan-class spread of the $k^{f_{\mathrm{clin}},f_{\mathrm{msr}}}_{Q_{\mathrm{clin}},Q_{\mathrm{msr}}}$ correction factors (expressed as a percentage). If this value is below 2% for a particular plan-class, the plan-class fulfills the criterion for a PCSR candidate plan. $\left|max\{k^{f_{\mathrm{clin}},f_{\mathrm{pcsr}}}_{Q_{\mathrm{clin}},Q_{\mathrm{pcsr}}}\}-1\right|$ refers to the maximum $k^{f_{\mathrm{clin}},f_{\mathrm{pcsr}}}_{Q_{\mathrm{clin}},Q_{\mathrm{pcsr}}}$ (expressed as a percentage relative to unity). The PCSR plan is representative of the plan-class if this value is below 2%. The correction factors for the non-isocentric field are taken at the optimal dose gradient metric point.

Plan-class name	$\left\|\Delta k^{f_{\mathrm{clin}},f_{\mathrm{msr}}}_{Q_{\mathrm{clin}},Q_{\mathrm{msr}}}\right\|$ (%)	Fulfill plan-class criterion (Y/N)	$\left\|max\{k^{f_{\mathrm{clin}},f_{\mathrm{pcsr}}}_{Q_{\mathrm{clin}},Q_{\mathrm{pcsr}}}\}-1\right\|$ (%)	Fullfill PCSR criterion (Y/N)
ISO-5mm	1.3%	Y	1.4%	Y
ISO-7.5mm	0.8%	Y	0.5%	Y
ISO-10mm	0.7%	Y	0.7%	Y
NONISO-TN1	0.8%	Y	10.2%	N
NONISO-TN2	1.1%	Y	11.1%	N
NONISO-AN1	3.1%	N	11.0%	N
NONISO-AN2	2.9%	N	6.6%	N

authors (Bouchard et al. 2009, Scott et al. 2012, Francescon, Beddar, Satariano & Das 2014). The large value of $[P_\rho]^{f_{\rm pcsr},f_{\rm msr}}_{Q_{\rm pcsr},Q_{\rm msr}}$ is due to the lack of lateral CPE in the small fields composing the clinical plans: the low-density cavity causes a large perturbation to the detector response (Bouchard et al. 2015). Conversely, the volume averaging correction factor is due to the highly non-uniform dose distribution in the small field across the detector sensitive volume. These two effects are more pronounced for the larger air cavity of the A26 micro chamber compared to the A16, resulting in larger total correction factors for the A26 than for the A16. Both of these intermediate correction factors decrease as the collimator diameter used in the clinical plan increases.

The correction factors for the W1 PSD were closest to unity compared to the other detectors. However, a 3% to 4% correction is still required for the plans using the 5 mm collimator, while $k^{f_{\rm clin},f_{\rm msr}}_{Q_{\rm clin},Q_{\rm msr}}$ for the plans using the larger collimators was within 0.5% of unity. Many authors (Wang & Beddar 2011, Francescon, Kilby & Satariano 2014, Papaconstadopoulos et al. 2014, Francescon, Beddar, Satariano & Das 2014) have calculated a correction factor within 1% of unity for the W1 for the 5 mm collimator, through a range of depths and off-axis positions. The discrepancy can be resolved by analyzing the intermediate correction factors. In the ISO-5mm PCSR plan, all intermediate correction factors except for $[P_{vol}]^{f_{\rm pcsr},f_{\rm msr}}_{Q_{\rm pcsr},Q_{\rm msr}}$ for the W1 PSD were calculated to be within 0.5% of unity, thanks to the use of water-equivalent materials throughout the scintillator's construction. This volume averaging effect was not observed by other authors, since in those studies the W1 was oriented with the long axis of the detector sensitive volume (which is 3 mm long and 1 mm in diameter) along the central axis of the field. In these clinical plans, however, individual fields can irradiate the long axis of the sensitive volume from virtually any angle.

4.2. Non-isocentric clinical plan-classes

The total correction factors, $k^{f_{\rm pcsr},f_{\rm msr}}_{Q_{\rm pcsr},Q_{\rm msr}}$, for the non-isocentric PCSR plans are much lower (2.4%-15%) than the $k^{f_{\rm clin},f_{\rm msr}}_{Q_{\rm clin},Q_{\rm msr}}$ correction factors for clinical plans and for all detectors. The total and intermediate correction factors for these homogenous plans do not agree well with those for heterogeneous clinical plans for any plan-class at either measurement point considered here, indicating that the chosen PCSR plans are not representative of the clinical plans in the respective class. This is likely due to the highly dissimilar dosimetric conditions between the PCSR plans and the clinical plans: whereas the PCSR plans were constructed to deliver a relatively homogeneous dose in a volume surrounding the detector, clinical plans had no such constraint, and instead were optimized according to the patient's anatomy.

The difference in dosimetric conditions between the PCSR and clinical plans is further demonstrated in the intermediate correction factors. The detector positions for these plans for plan-classes NONISO-TN2, AN1, and AN2 are all in a lower dose region surrounded by a larger region of high dose. The $[P_{vol}]^{f_{\rm pcsr},f_{\rm msr}}_{Q_{\rm pcsr},Q_{\rm msr}}$ factors for the scintillator detector are less than or equal to unity for these plans, consistent with the measurement position being at a low dose gradient or an approximate dose minimum. For all but one PCSR plan, the micro chamber $[P_\rho]^{f_{\rm pcsr},f_{\rm msr}}_{Q_{\rm pcsr},Q_{\rm msr}}$ and $[P_{vol}]^{f_{\rm pcsr},f_{\rm msr}}_{Q_{\rm pcsr},Q_{\rm msr}}$ are less than unity, while $[P_{wall}]^{f_{\rm pcsr},f_{\rm msr}}_{Q_{\rm pcsr},Q_{\rm msr}}$ is greater than unity unlike any of clinical plans considered here. This behaviour in the PCSR plans is in contrast to the usual expectations for small field correction factors that $[P_{vol}]^{f_{\rm clin},f_{\rm msr}}_{Q_{\rm clin},Q_{\rm msr}}$ $[P_\rho]^{f_{\rm clin},f_{\rm msr}}_{Q_{\rm clin},Q_{\rm msr}}$ should be less than unity (Das et al. 2008). Furthermore it has been shown (Papaconstadopoulos et al. 2014, Francescon, Beddar,

Satariano & Das 2014) that micro chambers over-respond in the penumbra and umbra of small fields. The difference in total correction factors for the PCSR plans may be due to the fact that more dose is contributed from the high-gradient and tail regions of the dose profiles, since a larger, more homogeneous dose volume is irradiated than for the clinical plans using the same sized collimators. This suggests that a PCSR plan that employs the same set of collimators as a given clinical plan but that delivers a uniform dose to a target is not necessarily dosimetrically representative of the clinical plans.

Even if a more suitable PCSR plan could be constructed, the intra-plan-class variation of $k_{Q_{\mathrm{clin}},Q_{\mathrm{msr}}}^{f_{\mathrm{clin}},f_{\mathrm{msr}}}$ for the micro chambers is too high to admit a possible PCSR plan for either micro chamber. The large intra-plan-class variation ($> 3\%$) of the $k_{Q_{\mathrm{clin}},Q_{\mathrm{msr}}}^{f_{\mathrm{clin}},f_{\mathrm{msr}}}$ correction factors for the larger A26 micro chamber in all but the NONISO-TN2 plan-class (variation 1.7%) precludes the application of the Alfonso formalism to this chamber for these specific plan-classes. For the smaller volume chamber, the variation is improved, with plan-classes NONISO-TN1 and NONISO-TN2 passing the 2% variation criterion laid out in the Materials and Methods, if the detector is placed at the optimal dose gradient metric point (see Table 5). At the maximum dose point, however, the variation in the latter plan-class worsens to 2.9%. The variation of the A16 correction factor within plan-class NONISO-AN1 is too high at both points considered: 3.1% at the optimal dose gradient metric point, and worsening to 3.5% at the maximum dose point. For plan-class NONISO-AN2, the situation is reversed, with variation improving to 1.9% at the maximum dose point, within the tolerance limit of 2%. Even if the contribution to the total plan from each collimator is considered separately, the variations in micro chamber $k_{Q_{\mathrm{clin}},Q_{\mathrm{msr}}}^{f_{\mathrm{clin}},f_{\mathrm{msr}}}$ do not meet the criterion (data not shown).

For the microchambers, this difference in behaviour between plan-classes when changing the point of measurement extends to the values of the correction factors themselves. For example, in plan-classes NONISO-TN2 and NONISO-AN1, $k_{Q_{\mathrm{clin}},Q_{\mathrm{msr}}}^{f_{\mathrm{clin}},f_{\mathrm{msr}}}$ generally decreases when moving from the optimal metric point to the maximum dose point, while it is increased for plans in NONISO-AN2. The reason for this difference is revealed by examining the volume averaging and density correction factors, shown in Figure 6. Plans in plan-classes NONISO-TN1, TN2, and AN1 exhibit the expected behaviour for these correction factors, that is, large and greater than unity. However, for plans in plan-class NONISO-AN2, which produced dose distributions in which the centre of the target receives less dose than the periphery, these two correction factors are much closer to 1, with $[P_{\mathrm{vol}}]_{Q_{\mathrm{pcsr}},Q_{\mathrm{msr}}}^{f_{\mathrm{pcsr}},f_{\mathrm{msr}}}$ even decreasing below unity for plan 1 at the optimal metric point. The volume averaging correction factor is determined by the dose distribution inside the sensitive volume of the detector. The irregular dose distribution for plans in plan-class NONISO-AN2 mean that the average dose inside the sensitive volume can be nearly equal to, or even greater than, the point dose at the centre, leading to a volume averaging correction close to or less than unity. These effects are even more pronounced for the PCSR candidate plans for plan-classes NONISO-TN2, AN1, and AN2.

The preceding analysis is applicable only if the chamber is placed in a region where dose is lower than the surrounding area; this is true of the optimal dose gradient metric point for plans 1 and 2 of plan-class NONISO-AN2. For plan 3, the optimal metric point was determined to lie in the high-dose periphery of the target, meaning that the volume averaging correction factor is much higher than the other plans. This can explain why the total correction factor is not changed significantly for this plan when moving between the two points: the optimal metric point and the

maximum dose point are both in a similar high-dose region. One can now see why the variation in $k_{Q_{\text{clin}},Q_{\text{msr}}}^{f_{\text{clin}},f_{\text{msr}}}$ is smaller at the maximum dose point than at the optimal metric point: all plans have the detector positioned in a similar region at the former point, while for plans 1 and 2 the latter point is in the central, low-dose region.

For most of the non-isocentric plans, the micro chamber density correction factor, $[P_\rho]_{Q_{\text{clin}},Q_{\text{msr}}}^{f_{\text{clin}},f_{\text{msr}}}$, is substantially greater than unity, reflecting a low-density material in a region with a lack of charged particle equilibrium (Scott et al. 2012). For plans 1 and 2 of plan-class NONISO-AN2 at the optimal dose metric point, this correction factor is much closer to unity (within 0.8-1.8%). This suggests that for this optimal metric point, the individual fields comprising the total clinical plan probably combine in such a way as to bring about a situation of approximate CPE at the detector position. This is true despite the fact that lateral CPE is never achieved in any singular field, as each one utilizes a small collimator. At the maximum dose point (and plan 3 in both points), the expected behaviour of lower CPE is restored, with the density correction factor between 3.4-5.2%.

For the W1, all plan-classes pass the $< 2\%$ $k_{Q_{\text{clin}},Q_{\text{msr}}}^{f_{\text{clin}},f_{\text{msr}}}$ variation criterion. Although the W1 detector requires additional corrections for Cerenkov light contamination (Guillot et al. 2011), it is nonetheless more simple to operate than other dosimeters which have been used for this purpose, including alanine, radiochromic film, and ferrous sulfate dosimetry, all of which require extensive pre-processing and/or readout procedures. This could permit the use of the PSD to directly measure the dose-to-water in non-isocentric clinical plans, or to measure $k_{Q_{\text{pcsr}},Q_{\text{msr}}}^{f_{\text{pcsr}},f_{\text{msr}}}$ correction factors for other detectors, taking note that care must be taken when performing measurements with any PSD to properly eliminate the Cerenkov signal from the raw reading in order to obtain the pure detector signal (Francescon, Beddar, Satariano & Das 2014).

5. Conclusions

Total and intermediate correction factors were calculated for 28 (21 clinical and 7 PCSR) CyberKnife plans employing the smallest collimators. Correction factors were calculated for three detectors: the A16 and A26 micro chambers, and the W1 PSD. Plans were grouped into plan-classes each having a PCSR plan sharing characteristics of the class that it represented. The suitability of using this PCSR plan as a representative plan for dosimetry was explored by calculating $k_{Q_{\text{pcsr}},Q_{\text{msr}}}^{f_{\text{pcsr}},f_{\text{msr}}}$ and $k_{Q_{\text{clin}},Q_{\text{pcsr}}}^{f_{\text{clin}},f_{\text{pcsr}}}$ correction factors.

For the isocentric plan-classes, a non-homogenous PCSR plan was determined to represent clinical plans at the 2% level for all detectors considered. For the non-isocentric plan-classes, micro chamber corrections could not be predicted using homogenous PCSR plans as proposed by Alfonso et al. (2008). For micro chambers, plan-classes for non-isocentric acoustic neuroma plans cannot even in principle be represented by any PCSR, as the variability in $k_{Q_{\text{clin}},Q_{\text{msr}}}^{f_{\text{clin}},f_{\text{msr}}}$ between different clinical plans and within the same plan at different measurement points is too high. The proposed method of grouping clinical plans into plan-classes, therefore, cannot reliably predict similar $k_{Q_{\text{clin}},Q_{\text{msr}}}^{f_{\text{clin}},f_{\text{msr}}}$ correction factors for these detectors. The $k_{Q_{\text{clin}},Q_{\text{msr}}}^{f_{\text{clin}},f_{\text{msr}}}$ correction factor for micro chambers depends on the collimator(s) used, anatomy treated, field path, homogeneity of the resulting dose distribution, and detector position within a specific plan.

Conversely, it has been shown that the W1 may be used to determine dose-to-water without correction for the measurement of the $k_{Q_{\text{clin}},Q_{\text{msr}}}^{f_{\text{clin}},f_{\text{msr}}}$ correction factor for CyberKnife small clinical plans

(isocentric and non-isocentric) not employing the 5 mm collimator. For plans employing the 5 mm collimator, only relatively simple corrections for volume averaging are required.

Acknowledgments

We acknowledge Carleton University for use of their computer cluster. Thanks also to Etienne Lessard and Warren Kilby from Accuray for useful discussion and for technical assistance. We appreciate helpful suggestions concerning beam modeling and assistance with `egs_chamber` from Frédéric Tessier. Thanks to Bernie Lavigne for assistance with the phantom specifications. EC acknowledges partial support by the CREATE Medical Physics Research Training Network grant of the Natural Sciences and Engineering Research Council (Grant number: 432290).

6. References

Alfonso R, Andreo P, Capote R, Huq M S, Kilby W, Kjäll P, Mackie T R, Palmans H, Rosser K, Seuntjens J, Ullrich W & Vatnitsky S 2008 *Medical Physics* **35**(11), 5179–5186.

Ali E S M 2016 *Medical Physics* **43**(8), 4939.

Ali E S M & Rogers D W O 2007 *Medical Physics* **34**(6), 2143–2154.

Almberg S S, Frengen J, Kylling A & Lindmo T 2012 *Medical Physics* **39**(1), 40–47.

Almond P R, Biggs P J, Coursey B M, Hanson W F, Huq M S, Nath R & Rogers D W O 1999 *Medical physics* **26**(9), 1847–1870.

Andreo P, Burns D T, Hohlfeld K, Huq M S, Kanai T, Laitano F, Smyth V G & Vynckier S 2000 Absorbed Dose Determination in External Beam Radiotherapy: an internation code of practice for dosimetry based on standards of absorbed dose to water Technical report International Atomic Energy Agency Vienna, Austria.

Azangwe G, Grochowska P, Georg D, Izewska J, Hopfgartner J, Lechner W, Andersen C E, Beierholm A R, Helt-Hansen J, Mizuno H, Fukumura A, Yajima K, Gouldstone C, Sharpe P, Meghzifene A & Palmans H 2014 *Medical physics* **41**(7), 072103.

Barrett J C & Knill C 2016 *Medical Physics* **43**(3), 1035–1044.

Bassinet C, Huet C, Derreumaux S, Brunet G, Chéa M, Baumann M, Lacornerie T, Gaudaire-Josset S, Trompier F, Roch P, Boisserie G & Clairand I 2013 *Medical physics* **40**(7), 071725.

Beddar A S, Mackie T R & Attix F H 1992*a* *Physics in Medicine and Biology* **37**(10), 1883–1900.

Beddar A S, Mackie T R & Attix F H 1992*b* *Physics in Medicine and Biology* **37**(10), 1901–1913.

Benedict S H, Yenice K M, Followill D, Galvin J M, Hinson W, Kavanagh B, Keall P, Lovelock M, Meeks S, Papiez L, Purdie T, Sadagopan R, Schell M C, Salter B, Schlesinger D J, Shiu A S, Solberg T, Song D Y, Stieber V, Timmerman R, Tomeé W A, Verellen D, Wang L & Yin F F 2010 *Medical Physics* **37**(8), 4078.

Benmakhlouf H, Sempau J & Andreo P 2014 *Medical physics* **41**(4), 041711.

Bouchard H, Seuntjens J, Carrier J F & Kawrakow I 2009 *Medical Physics* **36**(10), 4654–4663.

Bouchard H, Seuntjens J, Duane S, Kamio Y & Palmans H 2015 *Medical Physics* **42**(10), 6033–6047.

Buckley L A, Kawrakow I & Rogers D W O 2004 *Medical Physics* **31**(12), 3425–3435.

Chibani O & Ma C M C 2007 *Medical physics* **34**(4), 1206–1216.

Cranmer-Sargison G, Weston S, Evans J a, Sidhu N P & Thwaites D I 2012 *Physics in Medicine and Biology* **57**(16), 5141–5153.

Czarnecki D & Zink K 2013 *Physics in Medicine and Biology* **58**(8), 2431–44.

Das I J, Ding G X & Ahnesjö A 2008 *Medical Physics* **35**(1), 206–215.

Dieterich S, Cavedon C, Chuang C F, Cohen A B, Garrett J A, Lee C L, Lowenstein J R, D'Souza M F, Taylor D D J, Wu X & Yu C 2011 **38**(6), 2914–2936.

Ezzell G A, Galvin J M, Low D, Palta J R, Rosen I, Sharpe M B, Xia P, Xiao Y, Xing L & Yu C X 2003 **30**(8), 2089–2115.

Francescon P, Beddar S, Satariano N & Das I J 2014 *Medical Physics* **41**(10), 101708.

Francescon P, Cora S & Cavedon C 2008 *Medical Physics* **35**(2), 504–513.

Francescon P, Cora S & Satariano N 2011 *Medical Physics* **38**(12), 6513–6527.

Francescon P, Kilby W & Satariano N 2014 *Physics in Medicine and Biology* **59**(6), N11–N17.

Gago-Arias A, Antolin E, Fayos-Ferrer F, Simon R, Gonzalez-Castano D M, Palmans H, Sharpe P, Gomez F & Pardo-Montero J 2013 *Medical Physics* **40**(1), 011721.

Guillot M, Gingras L, Archambault L, Beddar S & Beaulieu L 2011 *Medical Physics* **38**(4), 2140–2150.

Kawrakow I 2000 *Medical physics* **27**(3), 485–498.

Kawrakow I & Rogers D W O 2000 The EGSnrcCode System: Monte Carlo Simulation of Electron and Photon Transport Technical report National Research Council of Canada Ottawa, Canada.

Kawrakow I, Rogers D W O & Walters B R B 2004 *Medical Physics* **31**(10), 2883–2898.

Ma C M, Li J, Deng J & Fan J 2008 *Journal of Physics: Conference Series* **102**, 012016.

Ma C M & Nahum A E 1993 *Medical physics* **20**(4), 1189–1199.

McEwen M, DeWerd L, Ibbott G, Followill D, Rogers D W O, Seltzer S & Seuntjens J 2014 *Medical physics* **41**(4), 041501.

McEwen M R 2010 *Medical physics* **37**(5), 2179–2193.

Moignier C, Huet C & Makovicka L 2014 *Medical Physics* **41**(7), 071702.

Muir B R & Rogers D W O 2010 *Medical Physics* **37**(11), 5939–5950.

Papaconstadopoulos P, Tessier F & Seuntjens J 2014 *Physics in Medicine and Biology* **59**(19), 5937–5952.

Ralston A, Liu P, Warrener K, McKenzie D & Suchowerska N 2012 *Physics in Medicine and Biology* **57**(9), 2587–2602.

Rogers D W O 2009 *in* D. W. O Rogers & J. E Cygler, eds, 'Clinical Dosimetry Measurements in Radiotherapy' Medical Physics Madison, WI pp. 137–146.

Rogers D W O, Faddegon B A, Ding G X, Ma C M, We J & Mackie T R 1995 *Medical Physics* **22**(5), 503–524.

Scott A J D, Kumar S, Nahum A E & Fenwick J D 2012 *Physics in Medicine and Biology* **57**(14), 4461–4476.

Sheikh-Bagheri D & Rogers D W O 2002 *Medical Physics* **29**(3), 379–390.

Wang L L W & Beddar S 2011 *Medical Physics* **38**(3), 1596–1599.

Wulff J, Zink K & Kawrakow I 2008 *Medical Physics* **35**(4), 1328–1336.